Arabian Journal for Science and Engineering (2018) 43:4855–4861
https://doi.org/10.1007/s13369-018-3191-5

RESEARCH ARTICLE - MECHANICAL ENGINEERING

A Ductile Damage Criterion for AISI 321 Austenitic Stainless Steel at Different Temperatures and Strain Rates

Mehdi Shaban Ghazani[1] · **Beitallah Eghbali**[2]

Received: 12 November 2017 / Accepted: 20 March 2018 / Published online: 26 March 2018

Abstract
In the present study, the variation of the critical ductile damage during hot deformation was investigated using hot compression testing and finite element simulation. Based on the obtained results, the critical ductile damage diagram was developed for AISI 321 austenitic stainless steel. Results showed that the value of critical damage is not constant during deformation in the temperature range of 800–1200 °C. It is also concluded that the critical ductile damage value is varied between 0.24 and 0.41 depending on hot deformation conditions. This means that, the critical ductile damage value is increased with increasing deformation temperature and decreased by increasing strain rate.

Keywords Hot compression deformation · Finite element simulation · Critical ductile damage · Failure · Austenitic stainless steel

1 Introduction

Manufacturing of high-performance and defect-free parts by the use of hot deformation processes such as hot forging and rolling depends significantly on the applied thermomechanical parameters during the production process. Deformation with high-temperature metal forming techniques not only changes the shape of the part to a desirable form, but also alters the microstructure of material and therefore leads to the substantial change in the flow stress during deformation [1]. So, in order to produce defect-free parts with the proper microstructure, deformation temperature and strain rate must be selected with care [2]. In the case of metallic materials with low stacking fault energy (SFE) like as austenitic stainless steels and copper alloys, dynamic recrystallization occurs during hot deformation even though the SFE is increased with increasing deformation temperature [3]. Dynamic recrystallization is a thermal activated metallurgical phenomenon in which the deformed microstructure is replaced with equiaxed dislocation-free grains by a set of nucleation and growth mechanisms [4]. As a result of dynamic recrystallization, the flow stress of material is changed in a trend similar to flow curve shown in Fig. 1.

As it is seen, at the beginning of deformation process, the flow stress increases rapidly and then reach to a peak value (σ_p) at a certain strain (ε_p). The presence of peak in the hot flow curve of materials demonstrates the occurrence of dynamic recrystallization [5]. After a peak strain, the hot flow stress level decreases continuously to a constant value which is called steady-state stress (σ_{ss}). Austenitic stainless steels usually show a dynamic recrystallization type flow behavior during hot deformation. Dynamic recrystallization is technologically important because it refines the final microstructure of workpiece and also decreases the load required for execution of the hot deformation process [6]. In the case of materials with strain hardening behavior, critical values of deformation parameters that lead to crack initiation and failure of component could be determined directly by conducting different mechanical examinations. But deformation conditions in which ductile fracture is initiated cannot be evaluated precisely because voids and cracks are formed inside deformed sample and propagated to outside regions [7]. Thus, providing an indirect method to determine the critical conditions for ductile failure is of great importance. As it is clear in Fig. 2, for evaluation of the amount of ductile damage, a cubic element is considered. In this case, δS is the area of X plane and δS_{Dx} is the total area of fractured regions

✉ Mehdi Shaban Ghazani
m_shaban@bonabu.ac.ir

[1] Department of Materials Science Engineering, University of Bonab, P.O. Box 5551761167, Bonab, Iran

[2] Department of Materials Science Engineering, Sahand University of Technology, P.O. Box 51335-1996, Tabriz, Iran

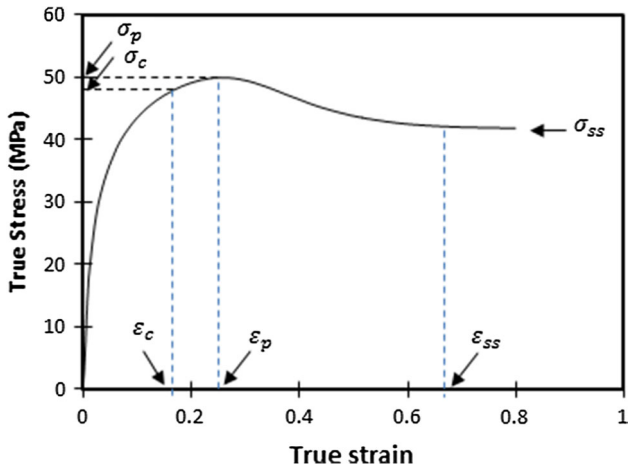

Fig. 1 True stress versus true strain curve during dynamic recrystallization

on X plane. Therefore, the amount of ductile damage at point M and in a direction perpendicular to X plane is evaluated according to the following equation [8]:

$$D(M.\vec{n}.x) = \frac{\delta S_{Dx}}{\delta S} \tag{1}$$

Different damage criteria were developed by researchers to investigate the ductile fracture behavior of materials. Craft–Latham damage criterion is the most important one [9,10]. As indicated in this model, the ductile fracture is initiated at a point inside workpieces when tensile strain energy exceeds a critical value. The Craft–Latham ductile damage value can be obtained using the following equation [11]:

$$D = \int_0^{\varepsilon_F} \frac{\sigma_T}{\bar{\sigma}} \mathrm{d}\bar{\varepsilon} \tag{2}$$

where ε_F is a fracture strain, σ_T is a maximum tensile stress, and $\bar{\sigma}$ is Von Mises equivalent stress value. It is inferred from this equation that the ductile damage value is increased with increasing plastic strain. Therefore, the maximum amount of damage factor is related to a moment of the initiation of voids at the end of defamation process. In order to investigate the trend of the variations of Craft–Latham damage during finite element simulation, the Craft–Latham damage sensitivity factor is introduced as follows [8]:

$$R_{\mathrm{Step}} = \frac{\Delta D}{D_{\mathrm{acc}}} \tag{3}$$

where ΔD is a variation of damage factor during specified step of simulation and D_{acc} is the cumulative amount of damage at the end of that step. The critical values of ductile damage for nonferrous alloys such as AZ80 magnesium [8] and Al7075 alloy [12] have been reported in literature, but there is no systematic investigation on ferrous alloys and stainless steels. Therefore, in the present study, the variation of critical ductile damage for AISI 321 austenitic stainless steel was obtained using hot compression deformation and finite element simulation at different temperatures and strain rates. The results can be used for determination of safe deformation conditions that can avoid ductile fracture during metal forming processes at high temperatures.

2 Material and Experimental Procedure

The chemical composition of the AISI 321 austenitic stainless steel used in the present study is shown in Table 1.

At first, cylindrical samples with 10 mm diameter and 15 mm length were prepared from as received rod. Afterward, the total number of 36 hot compression tests were con-

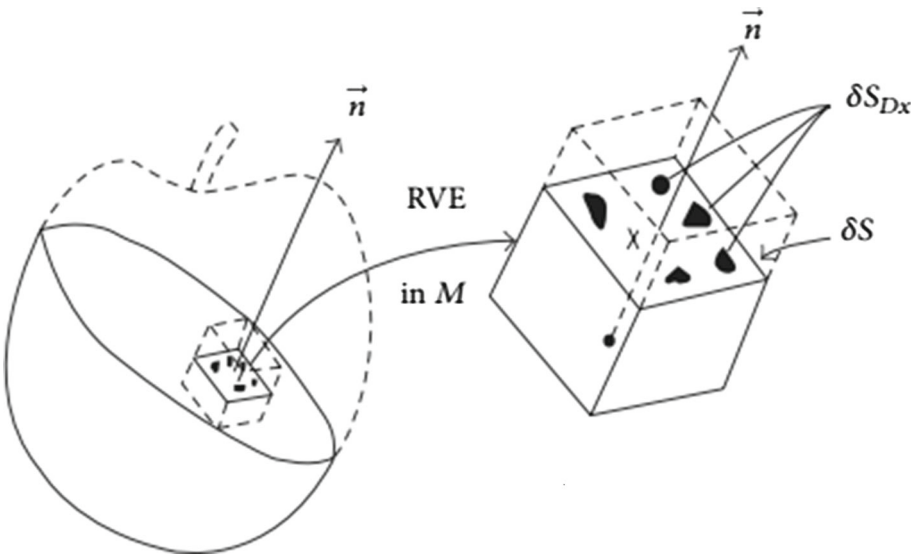

Fig. 2 Schematic representing the simple definition of damage [8]

Table 1 Chemical composition of the investigated steel

C	Si	Mn	Cr	Ni	Mo	Ti	Fe
0.04	0.36	1.873	18.16	10.52	0.24	0.32	Bal.

ducted over the temperature range of 800–1200 °C and strain rates in the range of 0.001–1 s^{-1} using Zwick–Roell Z250 testing machine and the hot flow curves were acquired by computer software. The force–displacement curves obtained from compression tests were converted to engineering stress–strain curves (S–e), and then the true stress–true strain curves (σ–ε) were calculated using the well-known equations ($\sigma = S(1-e)$, $\varepsilon = \ln(1-e)$). In the simulation, the Von Misses yield criterion was assumed and the material is considered as isotropic material. Also, the stress and strain fields are not uniaxial during compression test due to the existence of friction between sample and punches. Therefore, the flow curves must be corrected and the effect of stress triaxiality (increased flow stress level) must be removed from the obtained curves. In the present work, a classic formula to correct the effect of friction has been used, which is shown as follows [13]:

$$\bar{\sigma} = \frac{\sigma}{1 + \left(\frac{2}{3\sqrt{3}}\right) m \left(\frac{r_0}{h_0}\right) \exp\left(\frac{3\varepsilon}{2}\right)} \tag{4}$$

where $\bar{\sigma}$ is corrected flow stress, σ is true stress, and ε is true strain obtained directly from experimental data, m is friction coefficient calculated from the final shape of deformed samples, r_0 and h_0 are the initial radius and height of samples. Finite element simulation of hot compression deformation was performed by importing corrected experimental flow stress curves to DEFORM 3D V 10.2 software. Important parameters in the simulation procedure are deformation temperature, strain rate and the friction coefficient between sample and punches which are to be determined for achieving correct simulation results. Temperature and strain rate are constant during deformation process and are already defined for each simulation run. But the friction coefficient must be determined using a method that is explained later. For simulation of compression deformation, a cylindrical sample with dimensions similar to experimental sample (10 mm in diameter and 15 mm in length) was considered as deformable part and meshed with 10,000 tetrahedron elements. Upper and lower punches were assumed as rigid parts, and their temperature was set to deformation temperature. Also, the environment and sample temperatures and the punch speed were considered as experimental conditions.

3 Results and Discussions

3.1 Determination of Friction Coefficient

One of the most important parameters that affects the results of finite element simulation is the friction coefficient between workpiece and grips of compression testing machine. When frictionless condition is considered, the plastic strain distribution inside sample will be uniform. In such a condition, every element is deformed similar to the whole shape of the sample. As it is seen in Fig. 3, the presence of friction between sample and grips leads to barreling and non-uniform distribution of plastic strain inside sample.

The extent of barreling is attributed to the amount of friction between sample and punches. The following equation can be used for determination of friction coefficient from the final shape of the deformed sample [14]:

$$\mu = \frac{(R/h)\, b}{\left(4/\sqrt{3}\right) - \left(2b/3\sqrt{3}\right)} \tag{5}$$

where μ is friction coefficient, b is barreling coefficient, h is the height of sample after deformation, and R is an average radius. The average radius (R) is the radius of deformed sample after compression deformation in the frictionless conditions. The barreling coefficient (b) and average radius (R) can be obtained by the following equations [13]:

$$b = 4\left(\frac{R_M - R_T}{R}\right)\left(\frac{h}{h_0 - h}\right) \tag{6}$$

$$R = r_0\sqrt{\frac{h_0}{h}} \tag{7}$$

where r_0 and h_0 are initial radius and height of sample, and R_M and R_T are the maximum radius and upper radius of sample, respectively (see Fig. 3). Friction coefficients are obtained by the use of mentioned equations at different temperature and strain rates. Figure 4 shows the contour plot of

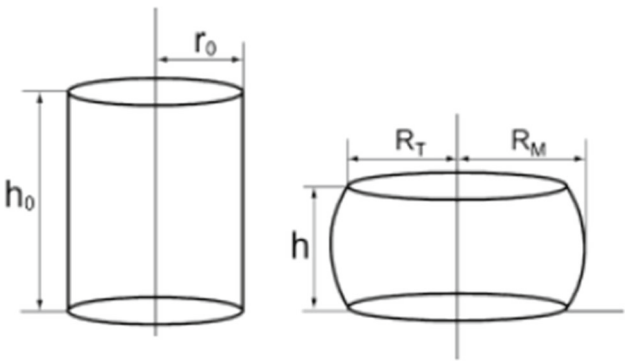

Fig. 3 Sample dimensions before and after hot compression

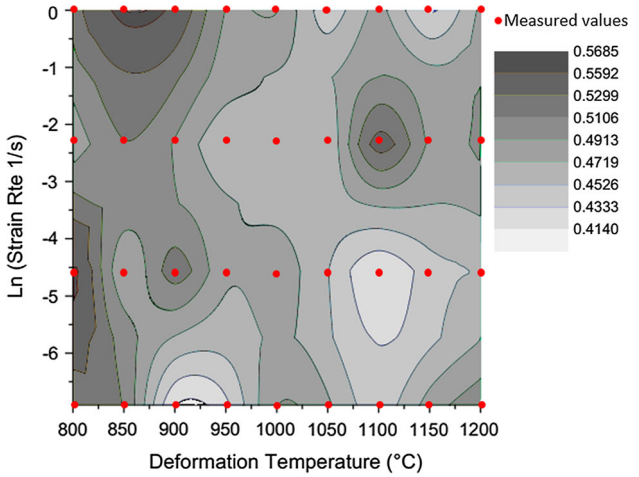

Fig. 4 Contour plot showing the effect of deformation temperature and strain rate on the magnitude of friction coefficient

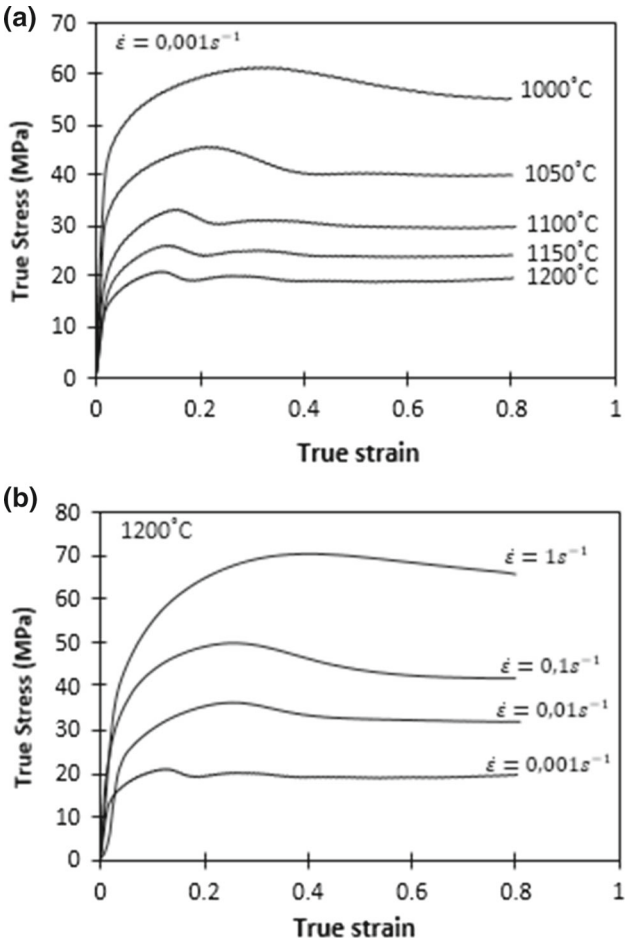

Fig. 5 Hot flow curves of AISI 321 stainless steel: **a** the effect of deformation temperature at constant strain rate of 0.001 s^{-1} and **b** the effect of strain rate at constant deformation temperature of 1200 °C

the variations of friction coefficients with deformation temperature and strain rate. As it is seen, the friction coefficient is varied with deformation conditions in the range of 0.41–0.58.

These variations can be attributed to the influence of deformation temperature and strain rate on flow stress of material through the occurrence of dynamic recrystallization or dynamic recovery. Accordingly, the variations in strength and hardness of material with temperature and strain rate can influence the friction between samples and punches. It is also worth noting that the small differences in the surface roughness of samples can also influence the friction coefficient. The non-monotonic variation of friction coefficient with temperature and strain rate is attributed to the effect of difference in the contact surface conditions between different samples and punches.

3.2 Hot Flow Curves

Figure 5 shows examples of hot flow curves of AISI 321 austenitic stainless steel obtained at different deformation conditions.

In Fig. 5a, the effect of deformation temperature at a constant strain rate of 0.001 s^{-1} is represented. Also, the effect of varying strain rate at constant deformation temperature of 1200 °C is shown in Fig. 5b. It is concluded that the flow stress of AISI 321 austenitic stainless steel is increased with decreasing deformation temperature and increasing strain rate. All hot flow curves show a similar trend. So that, flow stress increases rapidly at low strains and reaches to a maximum value that is the clear indication of the occurrence of dynamic recrystallization during hot deformation. Rapid increase in flow stress level at lower strains is explained by the work hardening of material due to generation and multiplication of dislocation [15]. The strain hardening rate is decreased by increasing strain that is a direct consequence of the increase in dynamic recovery rate. Dynamic recovery proceeds by annihilation and rearrangement of dislocation inside deformed grains [16]. All flow curves in Fig. 5 show a dynamic recrystallization type flow behavior. Although the presence of peak stress and strain in hot flow curve of material demonstrates the occurrence of dynamic recrystallization, this phenomenon occurs at lower strains which is denoted by ε_c (Fig. 1). The peak strain is achieved when the work hardening due to generation and multiplication of dislocations is fully compensated by the softening occurred as a result of dynamic recrystallization. Afterward, the flow stress decreases continuously to a steady-state value (σ_{ss}). The steady-state region is a consequence of the dynamic balance between work hardening and softening processes. In this stage of deformation, the grain size and dislocation density remain constant [17].

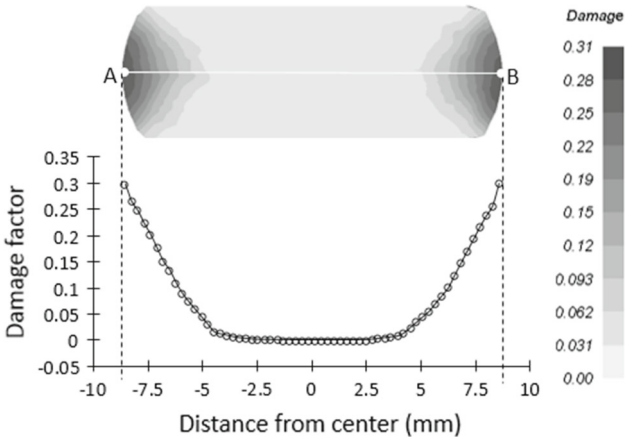

Fig. 6 Distribution of Craft–Latham damage inside deformed sample

3.3 Distribution of Craft–Latham Damage Factor

Figure 6 represents the distribution of Craft–Latham damage factor inside deformed sample at 800 °C and strain rate of 0.01 s^{-1}.

As it is seen, the damage factor is distributed non-uniformly. Also, the damage value at upper, lower and inner regions is considerably low and the maximum value is belonged to the peripheral regions of the middle of sample. Therefore, points *A* and *B* in Fig. 6 have a maximum damage value and ductile fracture may initiate from these regions. Therefore, the value of damage at these points is considered as critical damage that sample can sustain without fracture.

3.4 Effect of Temperature and Strain Rate on Critical Damage Value

Figure 7 shows the variations of the critical damage value with strain rate at different deformation temperatures.

It can be seen that the maximum damage factor decreases with increasing strain rate. In addition, damage factor is increased with deformation temperature at constant strain rate. Therefore, strain rate and deformation temperature have an opposing effect on the critical damage value. Also, it is concluded that the effect of strain rate on ductile damage value is more significant than the effect of deformation temperature. Therefore, the ductile fracture is more sensitive to strain rate than deformation temperature.

3.5 Deformation Conditions with Higher Risk of Ductile Fracture

Figure 8 illustrates the contour plot of the variation of ductile damage values with temperature and strain rate.

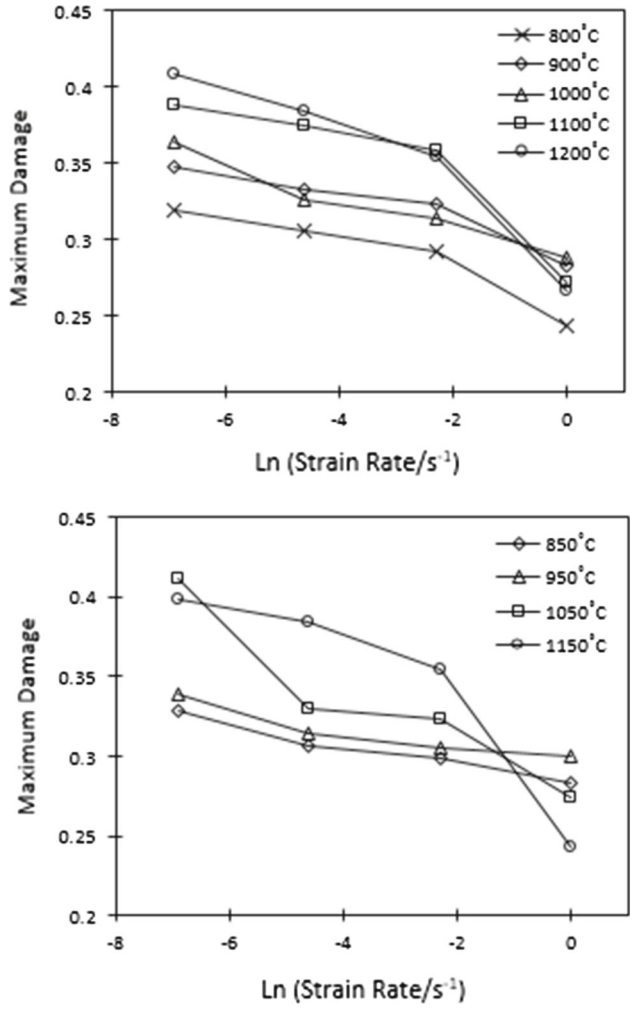

Fig. 7 Variation of maximum damage with strain rate at different deformation temperatures

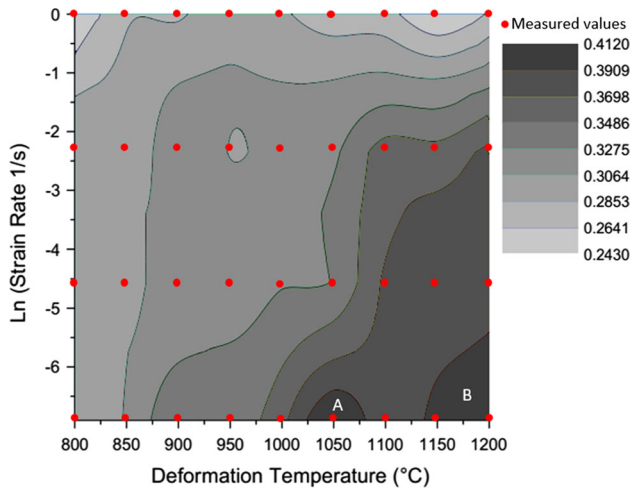

Fig. 8 A contour plot showing the effect of deformation temperature and strain rate on the magnitude of ductile fracture criterion

As can be seen, the ductile damage varies non-uniformly over the investigated temperature and strain rate ranges. Also, the minimum and maximum values are 0.24 and 0.41, respectively. The maximum value of ductile damage is located in regions marked by A and B letters. These regions correspond to deformation with strain rate of 0.001 s^{-1} in the temperature ranges of 1025–1075 and 1150–1200 °C, respectively, in which the dynamic recrystallization is a prevailing softening phenomenon. In addition, the minimum value for damage factor corresponds to strain rate of 1 s^{-1} both at low (region C) and high (region D) deformation temperatures. Region C corresponds to the deformation conditions where dynamic recovery is occurred. In contrast, region D coincides with conditions in which the dynamic recrystallization is initiated during deformation. From these observations, it can be concluded that at low strain rates the maximum amounts of damage can be tolerated by material that is due to the occurrence of dynamic recrystallization. But at high strain rates the minimum amounts of ductile damage are sustained. It is seen that the occurrence of dynamic recrystallization or dynamic recovery has no pronounced effect on the amount of tolerated ductile damage at high strain rates. It is also worth noting that the ductile fracture more likely to occur at deformation conditions corresponds to lower critical values of damage factor (regions C and D in Fig. 8).

4 Conclusions

In the present investigation, the critical ductile damage values of AISI 321 austenitic stainless steel were determined using hot compression deformation and finite element simulation. The following conclusions were attained:

1. Friction coefficient between sample and plunger is not constant over the investigated temperature and strain rate ranges.
2. Hot flow curves of AISI 321 austenitic stainless steel indicate the occurrence of dynamic recrystallization during deformation.
3. The Craft–Latham damage is not distributed uniformly inside sample. It has a minimum value at upper, lower and inner regions of sample. Also, the maximum value of damage factor is located at peripheral regions of the middle part of deformed sample.
4. The Craft–Latham damage increases with strain. The variations of damage are nonlinear at strains lower than 0.6, but it increases linearly at higher strains.
5. The maximum ductile damage is increased with increasing temperature and decreasing strain rate.
6. The contour plot obtained by finite element simulation shows that the maximum damage value is related to deformation with strain rate of 0.001 s^{-1} and temperature ranges of 1025–1075 and 1150–1200 °C. Therefore, these conditions have a lower risk of ductile fracture during metal forming processes.

References

1. Bontcheva, N.; Petzov, G.: Microstructure evolution during metal forming processes. Comput. Mater. Sci. **28**, 563–573 (2003). https://doi.org/10.1016/j.commatsci.2003.08.014
2. Reis, G.G.; Jorge, A.M.; Balancin, O.: Influence of the microstructure of duplex stainless steel on their failure characteristics during hot deformation. Mater. Res. **3**, 31–35 (2000). https://doi.org/10.1590/S1516-14392000000200006
3. Stewart, G.R.; Jonas, J.J.; Montheillet, F.: Kinetics and critical conditions for the initiation of dynamic recrystallization in 304 stainless steel. ISIJ Int. **44**, 1581–1589 (2004). https://doi.org/10.2355/isijinternational.44.1581
4. Jafari, M.; Najafizadeh, A.; Rasti, J.: Dynamic recrystallization by necklace mechanism during hot deformation of 316 stainless steel. Int. J. ISSI **4**, 16–23 (2007)
5. Shaban, M.; Eghbali, B.: Determination of critical conditions for dynamic recrystallization of a microalloyed steel. Mater. Sci. Eng. A **527**, 4320–4325 (2010). https://doi.org/10.1016/j.msea.2010.03.086
6. Samuel, F.H.; Yue, S.; Jonas, J.J.; Barnes, K.R.: Effect of dynamic recrystallization on microstructural evolution during strip rolling. ISIJ Int. **30**, 216–225 (1990). https://doi.org/10.2355/isijinternational.30.216
7. Dargon, A.: Plasticity and ductile fracture damage: study of void growth in metals. Eng. Fract. Mech. **21**, 875–885 (1985). https://doi.org/10.1016/0013-7944(85)90094-3
8. Yu, X.; Guo, Q.; Jie, Z.: Effect of temperature and strain rate on critical damage values of AZ80 magnesium alloy. Trans. Nonferrous Metal Soc. **20**, 580–583 (2010). https://doi.org/10.1016/S1003-6326(10)60542-0
9. Duan, X.; Velay, X.; Sheppard, T.: Application of finite element method in the hot extrusion of aluminium alloys. Mater. Sci. Eng. A **369**, 66–75 (2004). https://doi.org/10.1016/j.msea.2003.10.275
10. Bao, Y.; Wierzbicki, T.: A comparative study on various ductile fracture crack formation criteria. J. Eng. Mater. Trans. ASME **126**, 314–324 (2004). https://doi.org/10.1115/1.1755244
11. Figueiredo, R.B.; Cetlin, P.R.; Langdon, T.G.: The processing of difficult-to-work alloys by ECAP with an emphasis on magnesium alloys. Acta Mater. **55**, 4769–4779 (2007). https://doi.org/10.1016/j.actamat.2007.04.043
12. Quan, G.Z.; Wang, F.B.; Liu, Y.Y.; Shi, Y.; Zhou, J.: Evaluation of varying ductile fracture criterion for 7075 aluminum alloy. Trans. Nonferrous Met. Soc. China **23**, 749–755 (2013). https://doi.org/10.1016/S1003-6326(13)62525-X
13. Han, Y.; Qiao, G.; Sun, J.; Zou, D.: A comparative study on constitutive relationship of as-cast 904L austenitic stainless steel during hot deformation based on Arrhenius-type and artificial neural network models. Comput. Mater. Sci. **67**, 93–103 (2013). https://doi.org/10.1016/j.commatsci.2012.07.028
14. Li, Y.P.; Onodera, E.; Matsumoto, H.; Chiba, A.: Correcting the stress–strain curve in hot compression process to high strain level. Metall. Mater. Trans. A **40**, 952–990 (2009). https://doi.org/10.1007/s11661-009-9783-7
15. McQueen, H.J.: Development of dynamic recrystallization theory. Mater. Sci. Eng. A **387–389**, 203–208 (2004). https://doi.org/10.1016/j.msea.2004.01.064

16. Nes, E.; Marthinsen, K.; Brechet, Y.: On the mechanisms of dynamic recovery. Scr. Mater. **47**, 607–611 (2002). https://doi.org/10.1016/S1359-6462(02)00235-X

17. Derby, B.: Dynamic recrystallization: the steady state grain size. Scr. Metall. Mater. **27**, 1581–1586 (1992). https://doi.org/10.1016/0956-716X(92)90148-8